Biomedical Research (Tokyo) **38** (4) 257–267, 2017

Chronological immunolocalization of sclerostin and FGF23 in the mouse metaphyseal trabecular and cortical bone

Atsunaka Sakurai[1, 2], Tomoka Hasegawa[1], Ai Kudo[1, 3], Zhao Shen[1, 4], Tomoya Nagai[1, 5], Miki Abe[1], Taiji Yoshida[1], Hiromi Hongo[1], Tomomaya Yamamoto[1, 6], Tsuneyuki Yamamoto[1], Kimimitsu Oda[7], Paulo Henrique Luiz de Freitas[8], Minqi Li[9], Hidehiko Sano[2], and Norio Amizuka[1]

Departments of [1] Developmental Biology of Hard Tissue, [2] Restorative Dentistry, [3] Crown and Bridge Prosthodontics, [4] Oral and Maxillofacial Surgery, [5] Oral Functional Prosthodontics, Graduate School of Dental Medicine, Hokkaido University, Sapporo, Japan; [6] Self-Defense Force Hanshin Hospital; [7] Biochemistry, Niigata University Graduate School of Medical and Dental Sciences, Niigata, Japan; [8] Department of Dentistry, Federal University of Sergipe at Lagarto, Brazil; and [9] Shandong Provincial Key Laboratory of Oral Biomedicine, The School of Stomatology, Shandong University, Jinan, China

(Received 6 June 2017; and accepted 16 June 2017)

ABSTRACT

To assess the chronological participation of sclerostin and FGF23 in bone metabolism, this study tracked the immunolocalization of sclerostin and FGF23 in the metaphyses of murine long bones from embryonic day 18 (E18) through 1 day after birth, 1 week, 2 weeks, 4 weeks, 8 weeks, and 20 weeks of age. We have selected two regions in the metaphyseal trabeculae for assessing sclerostin and FGF23 localization: close to the chondro-osseous junction, *i.e*., bone modeling site even in the adult animals, and the trabecular region distant from the growth plate, where bone remodeling takes place. As a consequence, sclerostin-immunopositive osteocytes could not be observed in both close and distant trabecular regions early at the embryonic and young adult stages. However, osteocytes gradually started to express sclerostin in the distant region earlier than in the close region of the trabeculae. Immunoreactivity for FGF23 was observed mainly in osteoblasts in the early stages, but detectable in osteocytes in the later stages of growth in trabecular and cortical bones. *Fgf23* was weakly expressed in the embryonic and neonatal stages, while the receptors, *Fgfr1c* and *αKlotho* were strongly expressed in femora. At the adult stages, *Fgf23* expression became more intense while *Fgfr1c* and *aKlotho* were weakly expressed. These findings suggest that sclerostin is secreted by osteocytes in mature bone undergoing remodeling while FGF23 is synthesized by osteoblasts and osteocytes depending on the developmental/growth stage. In addition, it appears that FGF23 acts in an autocrine and paracrine fashion in fetal and neonatal bones.

By establishing a communication network between osteocytes and osteoblasts, osteocytes are situated at the center of bone turnover and help determine how bones adjust to mechanical stress through bone remodeling. Osteocytes exist inside osteocytic lacunae and connect to neighboring osteocytes and osteoblasts on the bone surfaces via fine cytoplasmic processes that run through osteocytic canaliculi. Osteocytes interconnect their cytoplasmic processes via gap junctions (2, 6, 7, 33), thereby building functional syncytia referred to as osteocytic lacunar-canalicular system (OLCS) (5, 15, 16, 31).

In the last few decades, many studies have reported on important osteocyte-derived factors, such as sclerostin (which regulates osteoblastic activities) and fibroblast growth factor 23 (FGF23, which affects the proximal renal tubules to reduce serum

Address correspondence to: Dr. Tomoka Hasegawa, DDSc. Department of Developmental Biology of Hard Tissue, Graduate School of Dental Medicine, Hokkaido University, Kita 13 Nishi 7 Kita-ku, Sapporo, 060-8586, Japan
Tel & Fax: +81-11-706-4226
E-mail: hasegawa@den.hokudai.ac.jp

concentrations of inorganic phosphate). Sclerostin is a glycoprotein encoded by the *Sost* gene (42) that binds to the LRP5/6 receptor—thereby antagonizing Wnt signaling and increasing β-catenin degradation (20, 40). Hence, sclerostin is known as a negative regulator of osteoblastic activity and bone remodeling (28, 35, 39), since it passes through the osteocytic canaliculi and inhibits the activation of bone-lining osteoblasts. FGF23, on the other hand, binds to the FGFR1c/αklotho receptor complex in adult stages at the proximal renal tubules; it helps controlling serum phosphate concentrations, which are required for normal skeletal development as well as for preservation of bone integrity (29). Although *Fgf23* mRNA was found in several tissues (1, 21, 34), it was most abundantly expressed in bone (41). As a circulating growth factor, FGF23 inhibits phosphate reabsorption and $1\alpha,25(OH)_2D_3$ production in the kidney (22), thus acting on serum homeostasis of phosphate and calcium. In brief, sclerostin and FGF23 are secreted by osteocytes and appear to be involved in bone metabolism in adult stages, *i.e.,* are involved in normal bone remodeling and serum mineral balance.

Meanwhile, each part of a long bone has its own function: metaphyseal primary trabeculae are sites of bone modeling based on mineralized cartilage cores formed during endochondral ossification (3). Secondary trabeculae show bone remodeling mediated by cellular coupling between osteoclasts and osteoblasts (4, 9, 10, 12). Cortical bone is a mature, well-mineralized hard tissue that composes the outer wall of the long bone. OLCS distribution differs depending on such regional difference of bone (13, 31, 37). Immature, primary trabeculae contained randomly-oriented OLCS, revealing an intense tissue nonspecific alkaline phosphatase (TNAP)-reactivity, a hallmark of osteoblastic activities (3, 26), on their surface. In contrast, secondary trabeculae constructed relatively-regular OLCS, and mature cortical bone demonstrated geometrically well-arrangement of OLCS, featuring TNAP-positive flattened, bone-lining osteoblasts (11, 23, 37). Normal bone remodeling is well known to make bone structure better strengthened and arranged so as to be resist against the mechanical stress, and by means of bone remodeling, the distribution of OLCS becomes progressively more regular as the individual grows. Therefore, the biological activities of osteocytes seem to take place in bone metabolism by means of specific molecules—sclerostin and FGF23 (11, 23, 37).

However, histological features of metaphyseal trabeculae and cortical bone chronologically change during individual growth, and therefore, the sites of bone modeling and remodeling will be different in accordance with the developmental stages (8). Kobayashi *et al.* have demonstrated that bone modeling mainly took place in tibiae, femora and vertebrates in the embryonic and infant stages of individual growth, whereas bone remodeling gradually came to be predominant in these bones after young adult stages (17). Thus, two important points were raised on the investigation of sclerostin and FGF23: One is that the embryonic and neonatal stages show mainly bone modeling in long bone, while bone remodeling would be predominant after young adult stage, and the other is the synthesis of sclerostin and FGF23 featuring the site-specific diversity of their immunolocalization.

Taken together, one may wonder whether there is a chronological change in the distribution of sclerostin-, or FGF23-immunoreactive osteocytes. To assess this concern, we have selected two regions of the metaphyseal trabeculae for sclerostin observation: the region close to the chondro-osseous junction (a bone modeling site even in young adults) and the region distant from the trabecular borders (bone remodeling is gradually predominant). In addition, we selected the region near the metaphyseal trabeculae as well as the cortical bone for FGF23 observation. The goal of this study, therefore, is to present the chronological changes in immunolocalization of sclerostin and FGF23 in the different regions of murine long bones during development and growth.

MATERIALS AND METHODS

Animals and tissue preparation. All animal experiments in this study were conducted under the Hokkaido University Guidelines for Animal Experimentation (Approved No. 15-0041). C57BL/6J mice at embryonic day 18 (E18), 1 day after birth, 1 week, 2 weeks, 4 weeks, 8 weeks, and 20 weeks of age (CLEA Japan Tokyo, Japan) were used in this study ($n = 6$ for each). E18 fetuses were obtained by Caesarean section, and then, immediately extracted and immersed in 4% paraformaldehyde in a 0.1 M phosphate buffer (pH 7.4). One day-old, 1 week-old and 2 weeks-old mice were anesthetized with diethyl ether and then, had their femora and tibiae extracted prior to being immersed in the same fixatives. Four weeks-old, 8 weeks-old, and 20 weeks-old mice were anesthetized with an intraperitoneal injection of 8% chloral hydrate (400 mg/100 g body weight). After the procedure, mice were performed with a trans-cardiac perfusion with 4% paraformaldehyde

in a 0.1 M phosphate buffer (pH 7.4) through left ventricles. These specimen were decalcified with 10% EDTA-2Na solution for 6 weeks at 4°C. After demineralization, the specimens were dehydrated through an ascending ethanol series prior to paraffin embedding.

Immunohistochemistry for sclerostin, FGF23 and TNAP. Dewaxed paraffin sections were treated with 0.1% hydrogen peroxide for 15 min. After pre-incubation with 1% bovine serum albumin (BSA; Serologicals Proteins Inc. Kankakee, IL) in PBS (1% BSA-PBS) for 30 min at room temperature (RT), the treated paraffin sections were incubated with rabbit polyclonal antisera against TNAP (26) at a dilution of 1 : 500 with 1% BSA-PBS at RT. These sections were reacted with horseradish peroxidase (HRP)-conjugated goat anti-rabbit IgG (DakoCytomation, Glostrup, Denmark), proceeded rinsing with PBS. For detection of FGF23 and sclerostin, the dewaxed paraffin sections were treated with rat anti-FGF23 (R&D systems, Inc., Minneapolis, MN) diluted at 1 : 100 for 2 h at RT, or with goat anti-mouse sclerostin antibody (R&D systems) at a dilution of 1 : 100 for 2 h at RT, respectively. Sections treated with primary antibodies were subsequently incubated in HRP-conjugated anti-rat IgG (Chemicon International Inc., Temecula, CA) or in HRP-conjugated anti-goat IgGs (Rockland Immunochemicals Inc., Gilbertsville, PA) at a dilution of 1 : 100 at RT. All immune complexes were visualized using 3,3'-diaminobenzidine tetrahydrochloride (DAB; Dojindo Laboratories, Kumamoto, Japan). All sections were counterstained with methyl green, and observed under light microscope (Eclipse E800; Nikon Instruments Inc. Tokyo, Japan).

The measurement of the indices of sclerostin-reactive osteocytes, FGF23-positive osteocytes and osteoblasts and TNAP-immunoreactive area. The percentage of sclerostin-positive osteocytes per total osteocyte number was examined in the close and distant regions from the chondro-osseous junction of tibiae at E18-, 1 day-, 1 week-, 2 weeks-, 4 weeks-, 8 weeks-, and 20 weeks-old mice ($n = 6$ for each). The region of interesting (ROI) close to the chondro-osseous junction was defined as the putative area encompassed by the chondro-osseous junction, endosteal surfaces of the cortical bone and the line placed at the first quarter of the length of the metaphyseal trabeculae starting from the chondro-osseous junction. In contrast, the ROI in the distant region of the metaphyseal trabeculae was defined as the area comprised by the last quarter of the metaphyseal trabeculae and the endosteal surfaces of the cortical bone. The numbers of sclerostin-immunoreactive osteocytes were divided by the total osteocyte number in the ROI.

Regarding the index of FGF23-immunopositive osteocytes, we have evaluated the percentage of FGF23-positive osteocytes per total osteocyte number in the ROI near the chondro-osseous junction and the cortical bone in all stages of mice growth and development stages included in this study ($n = 6$ for each). The ROI of the close region is described above, and that of cortical region was estimated by the area encompassed by assumed two extensive lines of the chondro-osseous junction and the one fourth of the trabecular length, and endosteal and periosteal surfaces. The numbers of FGF23-immunoreactive osteocytes were divided by the total numbers of osteocytes in the ROI. We measured the osteoblastic areas positive for FGF23 in the cortical area, by using ImagePro Plus 6.2 software (Media Cybernetics, Silver Spring, MD) and represented as percentage of tissue volume (TV) as recently reported (43).

TNAP-positive areas within the ROI of the close and distant region described above were also measured with using ImagePro Plus 6.2 software (Media Cybernetics), and the resulting indices were statistically analyzed and described in terms of percentage of TV.

Statistical analysis. All statistical analyses were assessed by one-way ANOVA followed by Tukey-Kramer multiple comparisons test, and all values are presented as mean ± standard deviation (SD). Values of $P < 0.05$ were considered significant (14, 36).

RT-PCR analysis for the expression of Fgf 23, Fgfr1c, αKlotho and Gapdh in femora and kidney. To evaluate the gene expression of *Fgf 23*, *Fgfr1c*, *αKlotho* and *Gapdh*, total RNA was extracted from femora and kidneys as previously reported (11). The specimens were homogenized in 10 mL TRIzol reagent (Life Technologies Co. Carlsbad, CA) per 1 g tissue to extract total RNAs. The mixture was centrifuged at 15,000 rpm for 5 min at 4°C, allowing for removal of small debris. The supernatant was transferred to a new tube, which was vortexed for 15 s after addition of 2 mL of chloroform. The lysate was then transferred to a new tube and incubated for 5 min at RT. After phase separation, the aqueous phase containing the RNA was transferred to a fresh new tube and RNA was precipitated by adding 5 mL isopro-

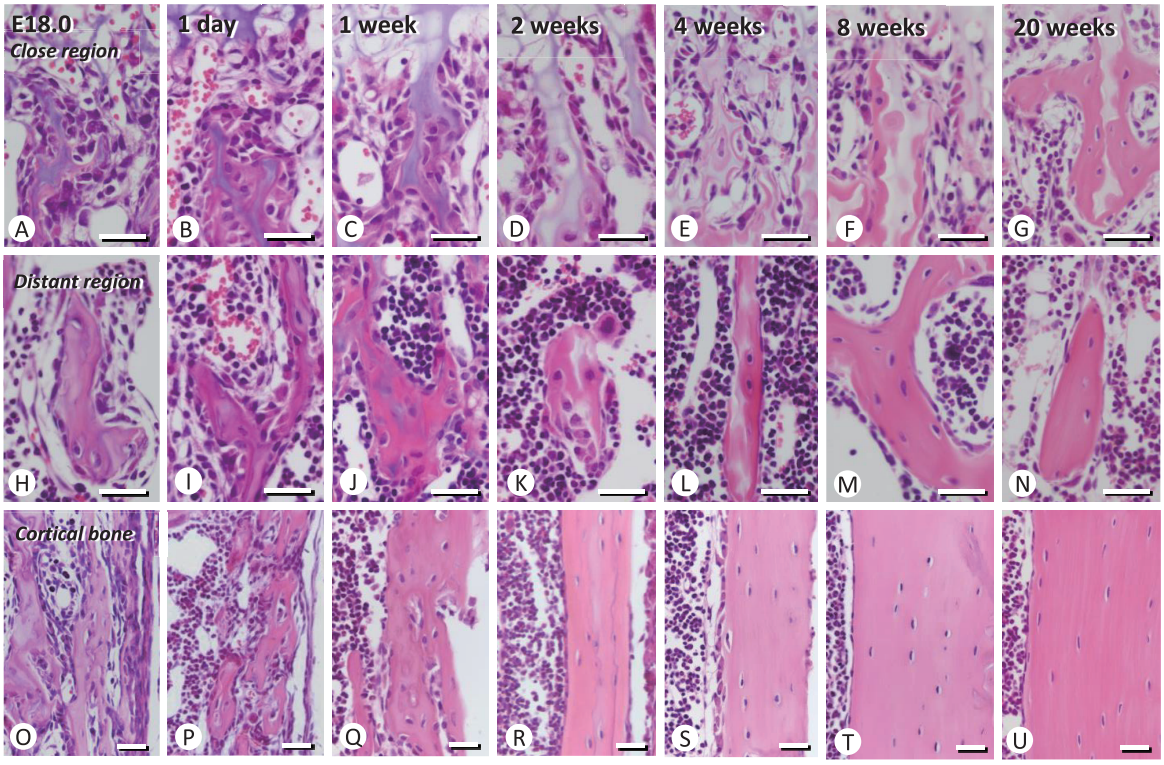

Fig. 1 Histology on the chronological change of metaphyseal trabeculae and cortical bone. Panels A–G display tibial trabeculae close to the chondro-osseous junction at E18 (A), 1 day (B), 1 week (C), 2 weeks (D), 4 weeks (E), 8 weeks (F), and 20 weeks (G)-old mice, while panels H–N and O–U are obtained from the distant regions of metaphyseal trabeculae and cortical bone, respectively, of the age-matched mice as panels A–G. Notice that, as mice grow, both trabeculae close to and distant from the chondro-osseous junction show compact profile with featuring flattened osteocytes. Although the cortical bone at E18 and 1 day after birth demonstrated gathering of fine trabeculae, thereafter, the cortical bone forms thick walls with compact histological profile. *Bars*, 50 μm

pyl alcohol per 10 mL TRIzol reagent. After 10 min incubation at RT, the mixture was centrifuged for 60 min at 15,000 rpm at 4°C. The resultant RNA pellet was washed with 1 mL 75% ethanol and briefly air-dried. RNA was dissolved in 30 μL DEPC-treated water. First strand cDNA was synthesized from 2 μg of total RNA by SuperScript VlLO cDNA Synthesis Kit (Life Technologies).

The primer sequences used for PCR were: mouse *Gapdh* Fw–TGTCTTCACCACCATGGAGAAGG, Rev–GTGGATGCAGGGATGATGTTCTG; mouse *Fgf23* Fw–TGTCAGATTTCAAACTCAG, Rev–GGATAGGCTCTAGCAGTG; mouse *Fgfr1c* Fw–CTTGACGTCGTGGAACGATCT, Rev–AGAACG GTCAACCATGCAGAG; mouse *αKlotho* Fw–GGG TCACTGGGTCAATCT, Rev–GCAAAGTAGCCA CAAAGG.

The PCR was performed using a thermal cycler, as follows: denaturation at 94°C for 30 s, annealing at 60°C (for *Gapdh*), 55°C (for *Fgf23, Fgfr1c* and *αKlotho*) for 30 s, extension at 72°C for 30 s, and a final incubation at 72°C for 10 min. RT-PCR products were subjected to 2% agarose gel electrophoresis, stained with ethidium bromide, and detected using E-Gel Imager (Life Technologies). The intensity of PCR products was photographed by digital camera, and analyzed by image J 1.48 (U.S. National Institutes of Health, Bethesda, Maryland) (32).

RESULTS

Chronological histology of metaphyseal trabeculae close and distant from the chondro-osseous junction and cortical bone

The trabeculae close to the chondro-osseous junction revealed a woven bone-like appearance with inner cartilage cores from E18 through 2 weeks of age (Figs. 1A–D). The region near the chondro-osseous junction was thicker at 4 and 8 weeks (Figs. 1E, F), and the thick bone matrix of the trabeculae included flattened osteocytes at 20 weeks (Fig. 1G). The

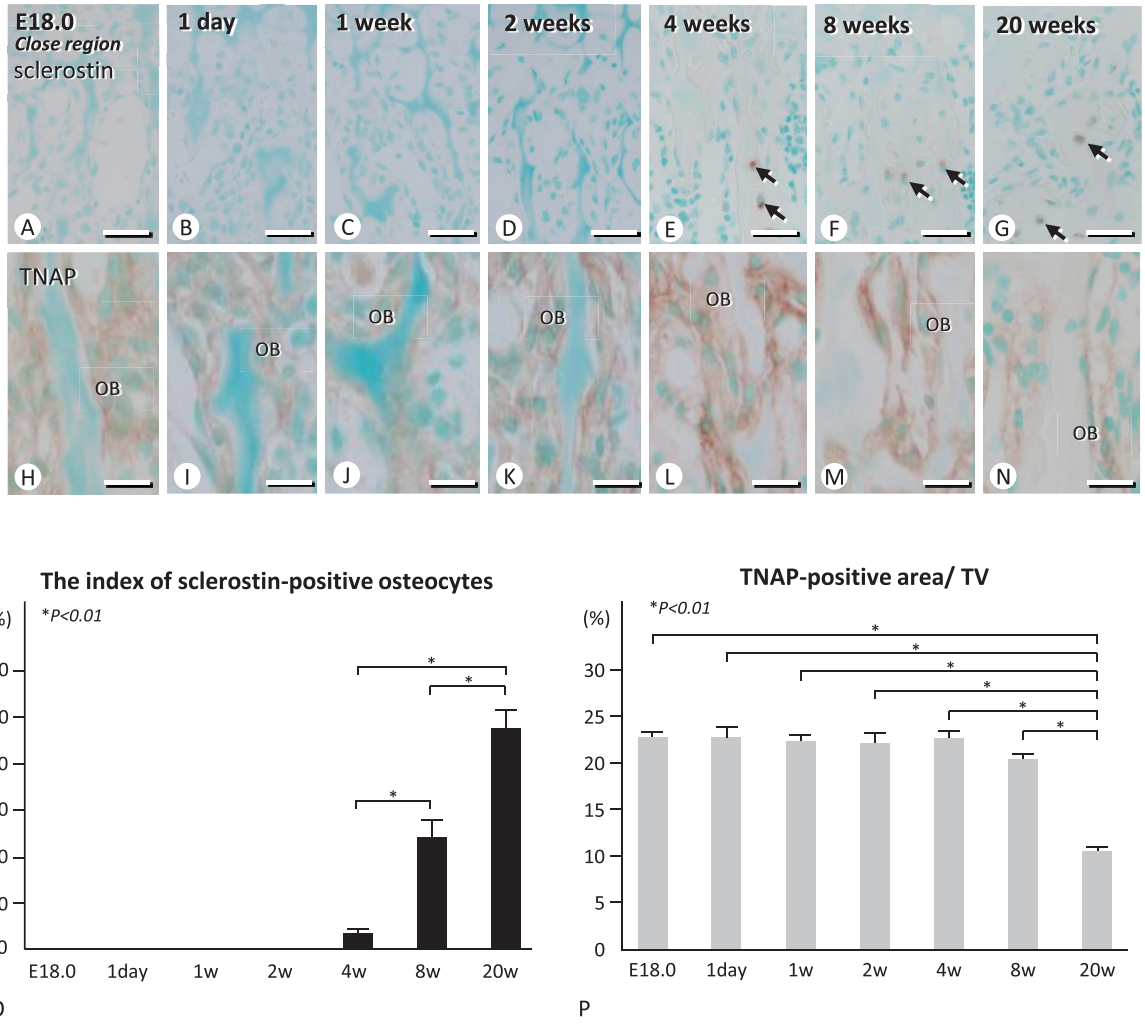

Fig. 2 Chronological distribution of sclerostin and TNAP in the metaphyseal trabeculae close to the chondro-osseous junction. Panels A–G display sclerostin-immunolocalization (brown) in trabeculae close to the chondro-osseous junction of tibiae at E18 (A), 1 day (B), 1 week (C), 2 weeks (D), 4 weeks (E), 8 weeks (F), and 20 weeks (G)-old mice, while panels H–N demonstrate the distribution of TNAP-reactive cells (brown color) in the matched region of A–G. See several osteocytes revealing sclerostin-immunoreactivity after 4 weeks (arrows in E–G). Panel O shows the statistical analysis on the index of sclerostin-reactive osteocytes in the trabeculae close to the chondro-osseous junction, while panel P exhibits the percentage of TNAP-positive area/TV. OB: osteoblast *Bars*, A–G: 50 μm, H–N: 20 μm

specimens at E18 and 1 day after birth revealed immature woven bone in the trabecular region distant from the chondro-osseous junction (Figs. 1H, I). However, starting from the first week of age, the distant region gradually thinned the layer of surrounding osteoblastic cells (Figs. 1J–L). The relatively flattened osteocytes were localized parallel to the trabecular surface after 8 weeks (Figs. 1M, N). The cortical bone at E18 and 1 day after birth was not a continuum of outer wall of bone, but demonstrated gathering of fine trabeculae (Figs. 1O, P). The cortical bone tended to form the cortical walls at 1 week-old (Fig. 1Q), and thereafter, exhibited thick walls with compact histological profile (Figs. 1R–U).

Sclerostin- and TNAP-immunolocalization in the metaphyseal trabeculae close and distant from the chondro-osseous junction

Since TNAP activity is a hallmark of osteoblastic cells, we compared the distribution of sclerostin and TNAP in the trabecular regions close and distant from the chondro-osseous junction. No sclerosin-positive osteocytes were observed in the trabeculae in the close proximity of the chondro-osseous junction from E18 to 2 weeks of age (Figs. 2A–D). At 4 weeks of age, the region near the chondro-osseous

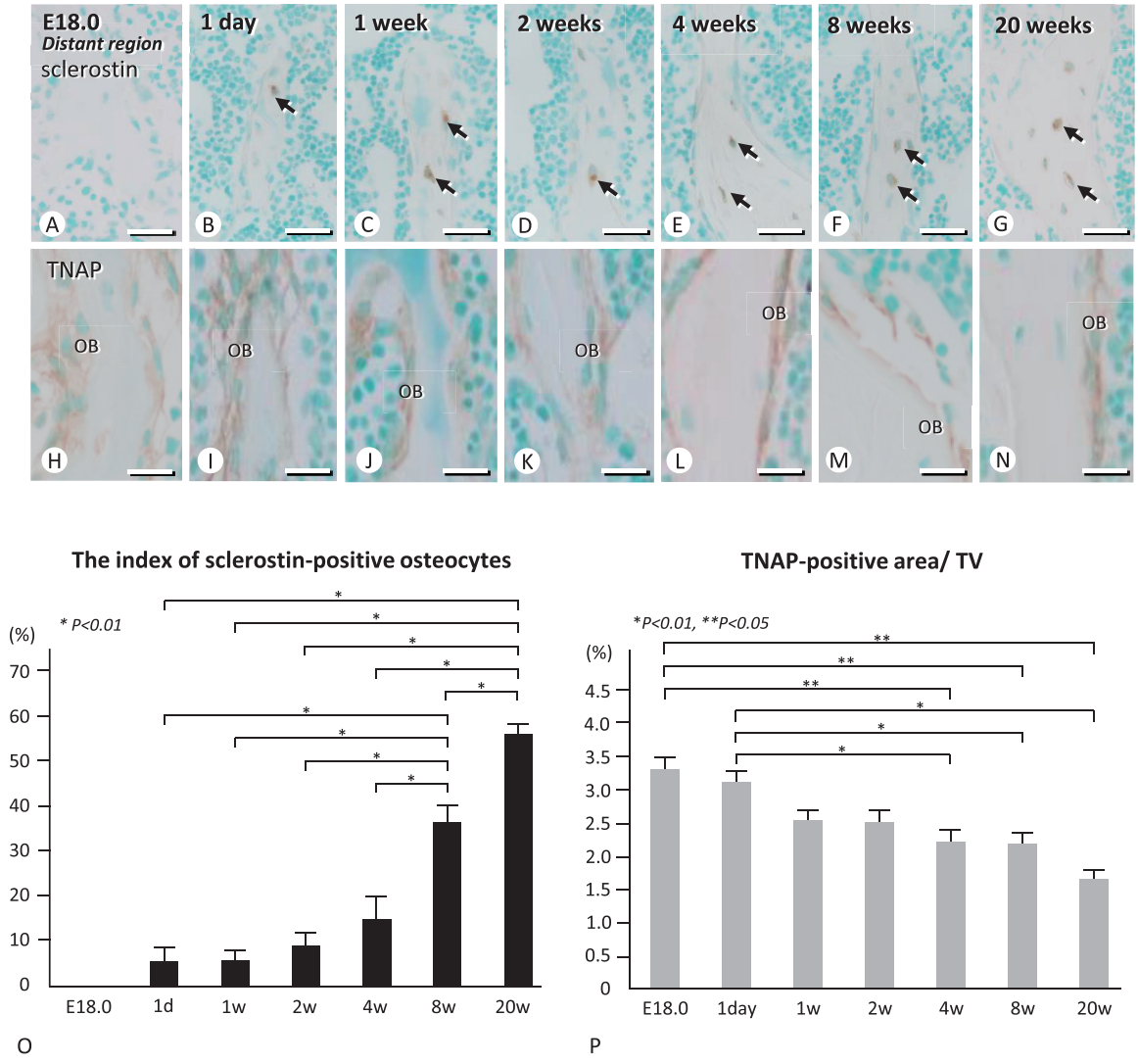

Fig. 3 Chronological distribution of sclerostin and TNAP in the metaphyseal trabeculae distant from the chondro-osseous junction. Panels A–G demonstrate the localization of sclerostin-immunoreactive osteocytes (brown color) in tibial trabeculae distant from the chondro-osseous junction at E18 (A), 1 day (B), 1 week (C), 2 weeks (D), 4 weeks (E), 8 weeks (F), and 20 weeks (G)-old mice, while panels H–N exhibit the distribution of TNAP-reactive cells (brown) in the matched region of panels A–G. Panel O is a graph of index of sclerostin-reactive osteocytes, while panel P shows the statistical analysis on the percentage of TNAP-positive area/TV. *Bars*, A–G: 50 μm, H–N: 20 μm

junction began to show sclerostin-immunoreactive osteocytes, with increasing numbers thereafter (Figs. 2E–G). Unlike sclerostin-immunolocalization, TNAP-reactive osteoblastic cell layers were very thick early at from E18 to 4 weeks-old of mice (Figs. 2H–L), began to decrease their thickness at around 8 weeks-old of age (Fig. 2M), and finally showed relatively-flattened profile at 20 weeks-old of age (Fig. 2N). Consistently, the percentage (mean ± SD) of sclerostin-immunopositive osteocytes in the close region was 3.65 ± 1.1 at 4 weeks-old, 24.66 ± 2.90 at 8 weeks-old, 48.74 ± 2.45 at 20 weeks-old of age (not detected from E18 to 2 weeks-old of age) (Fig. 2O). The statistical analyses exhibited the significant decrease of the index of TNAP positive area/tissue volume (TV) at 20 weeks-old when compared to that of the other stages (Fig. 2P).

In the distant trabecular region in the close proximity of the terminal end, the sclerostin-immunopositive osteocytes were not observable at E18 (Fig. 3A), but could be observable from 1 day after birth, and chronologically tended to increase their number (Figs. 3B–G). The statistical analysis on the index (mean ± SD) of sclerostin-positive osteocytes demon-

strated 5.66 ± 3.76 at 1 day, 5.80 ± 2.66 at 1 week-, 9.18 ± 3.58 at 2 weeks-, 15.12 ± 5.64 at 4 weeks-, 36.77 ± 4.25 at 8 weeks-, and 56.50 ± 2.51 at 20 weeks-old of age (not detected at E18) (Fig. 3O). As mice grow, TNAP-immunoreactive areas appear to be chronologically reduced (Figs. 3H–N), and consistently, the index of TNAP-positive area/TV was gradually attenuated in a linear gradient manner (Fig. 3P).

Chronological change of FGF23-immunolocalization in the trabeculae close to the chondro-osseous junction and cortical bone

From E18 to 1 day-old of age, FGF23-immunoreactivity was observed mainly in osteoblasts and preosteoblastic cells, rather than osteocytes in the close region to the chondro-osseous junction (Figs. 4A, B). Both osteoblasts and osteocytes were positive for FGF23-immunoreactivity at around 1 or 2 weeks-old (Figs. 4C). Thereafter, osteocytes rather than osteoblasts predominantly showed the FGF23-immunopositivity, though osteoblasts still showed the weak immunoreactivity (Figs. 4D–G). Coincidently, many osteoblasts and preosteoblastic cells in the cortical bone were immunoreactive for FGF23 at from E18 to 1 week-old (Figs. 4H–J), but after around 2 weeks, osteocytes predominantly revealed an intense FGF23-reactivity until 20 weeks-old of age (Figs. 4K–N). The immunolocalization of FGF23 in the distant trabecular region tended to appear as similar as those of the cortical bone (data not shown). The statistical analysis displayed that the indices (mean ± SD) of FGF23-positive osteoblasts as 21.92 ± 0.43 at E18, 20.50 ± 0.62 at 1 day-, 15.04 ± 0.39 at 1 week-, 8.04 ± 0.27 at 2 weeks-, 4.94 ± 0.23 at 4 weeks-, 1.32 ± 0.26 at 8 weeks-, and 1.02 ± 0.25 at 20 weeks-old of age, while those of FGF23-reactive osteocytes were 5.25 ± 0.17 at 1 week, 33.95 ± 0.31 at 2 weeks, 34.48 ± 0.34 at 4 weeks, 40.62 ± 0.26 at 8 weeks, and 46.07 ± 0.33 at 20 weeks of age in the cortical bone (not detected from E18 to 1 day-old of age) (Fig. 4O).

Chronological gene expression of Fgf23, Fgfr1c, αKlotho in femora and kidney

RT-PCR analyses using femoral specimens demonstrated the gene expression of *Fgf23* slightly in the E18 and 1 day after birth, and from 1 week-old, and thereafter, gradually became intense (Fig. 5A). Interestingly, genes encoding *Fgfr1*c and *αKlotho*, the molecules of which form the receptor complex for FGF23, were intensely expressed at from E18 to 1 or 2 weeks-old of age, and then chronologically reduced the intensity at 8 or 20 weeks of age (Fig. 5B). Unlike femora, the expression level of *Fgfr1*c and *αKlotho* in the kidney was constant during the experimental periods (Fig. 5C). The ratio of each gene expression standardized to *Gapdh* was shown in Fig. 5D, featuring the chronological decrease of *Fgfr1*c and *αKlotho* genes, but the gradual increment of *Fgf23* in femora.

DISCUSSION

In this study, we have examined the chronological localization of sclerostin and FGF23 in long bone, and obtained following findings.

1) Sclerostin is synthesized in osteocytes of the distant trabecular region earlier than the close region to the chondro-osseous junction.
2) FGF23 is produced mainly in osteoblasts in the early stage, but comes to be seen predominantly in osteocytes in the later stages of metaphyseal trabeculae and cortical bones.
3) Despite a weak expression of *Fgf23* mRNA, *Fgfr1c* and *αKlotho* are strongly expressed in the bone at the embryonic and neonatal stages. At the adult stage, *Fgf23* expression becomes intense, while *Fgfr1c/αKlotho* mRNAs are reduced.

Sclerostin and FGF23 have been known as osteocyte-derived factors (22, 28, 35, 39, 41, 42). However, this study revealed the different distribution of sclerostin/FGF23 between the close and distant regions of metaphyseal trabeculae. It seems of interest that FGF23-producing cells were changed from osteoblasts in the early stage into osteocytes in the later stage of mice development. Another importance is the reciprocal expression of *Fgf23* and *Fgfr1c*/*αKlotho* between the fetal/neonatal stages and adult stages, as shown in Figs. 4 and 5. These findings indicates the assumed autocrine/paracrine action of osteoblast-derived FGF23 in fetal/neonatal bones, although many literatures have suggested that FGF23/αklotho signaling serves for the systemic regulation of serum phosphate in adult kidney (18, 19, 24, 25, 38). Thus, our study apparently shows new insights on the chronological localization of sclerostin and FGF23 in bone in accordance with the developmental stages, and therefore, providing a clue for better understanding on which cells would synthesize these molecules during the developmental stages.

As shown in Figs. 2 and 3, one may could see a tendency that as sclerostin-positive osteocytes in-

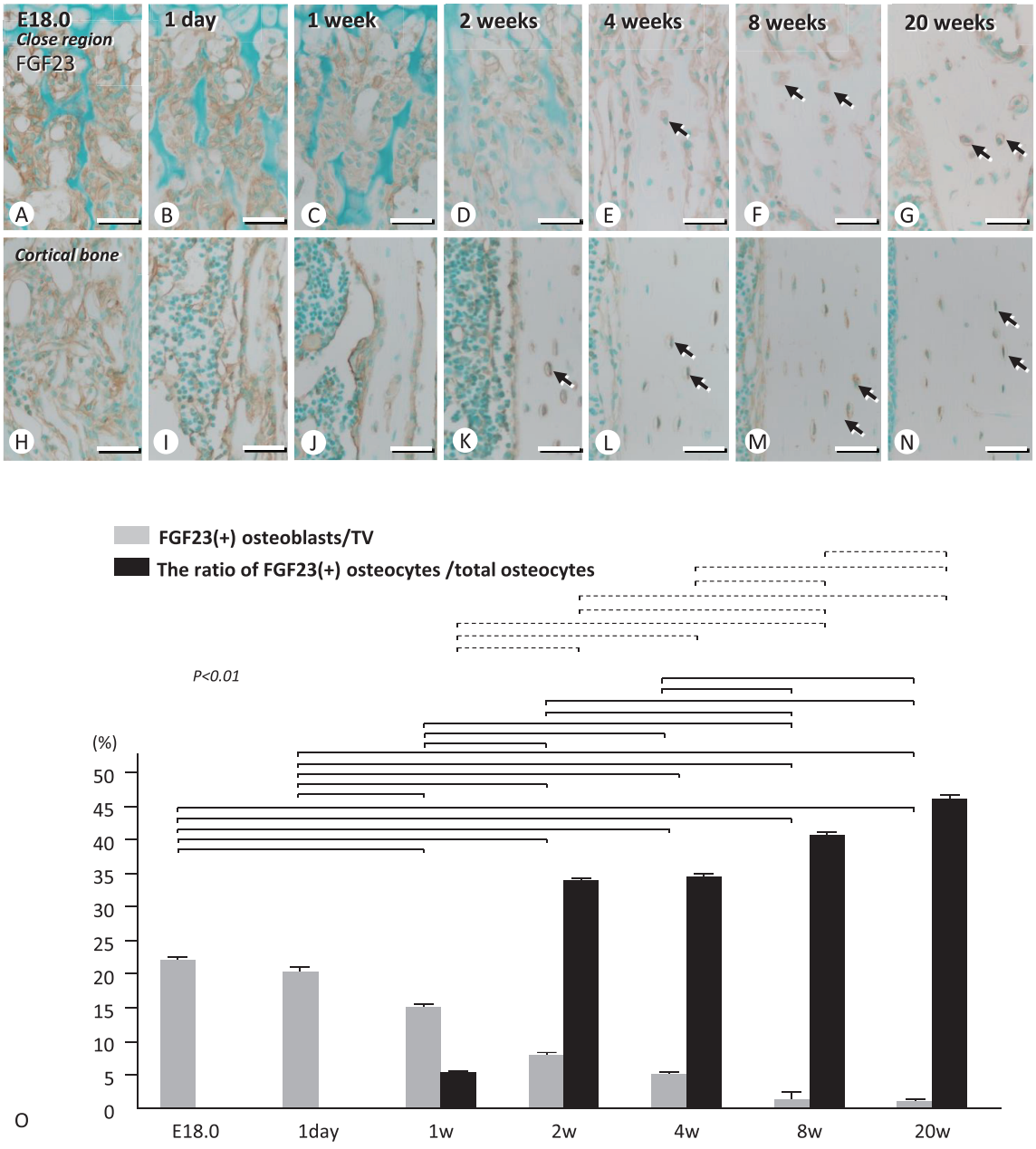

Fig. 4 Chronological change of FGF23-immunolocalization in the primary trabeculae and cortical bone. Panels A–G show the immunolocalization of FGF23-positive cells (brown color) in trabeculae in the close proximity of the chondro-osseous junction at E18 (A), 1 day (B), 1 week (C), 2 weeks (D), 4 weeks (E), 8 weeks (F), and 20 weeks (G)-old mice. Panels H–N reveal the distribution of FGF23-reactive cells (brown) in the cortical bones with the matched ages of A–G. Note that osteoblastic cells surrounding the trabeculae are main FGF23-immunoreactive cells (brown color) until 1 or 2 weeks after birth (A–D, H–J), but thereafter, osteocytes show intense immunoreactivities of FGF23 (arrows, E–G, K–N) in both metaphyseal trabeculae and cortical bones. Panel O reveals the statistical analysis on the indices of FGF23-positive osteoblasts and osteocytes. Note that fetal and neonatal stages show the predominant FGF23-immunopositivity of osteoblasts, while the adult stages reveal that osteocytes are main cells for the FGF23-positivity. Straight lines and dotted lines indicate the comparison on the indices of FGF23-positive osteoblasts and the ratio of FGF23-positive osteocytes/total osteocytes. *Bars*, 50 μm

creased, so TNAP-reactive areas/TV reduced in both the close and distant trabecular region. However, there was a slight difference in the chronological change of the sclerostin-positive osteocytes between the close and distant regions. The trabeculae close to the chondro-osseous junction displayed a broad

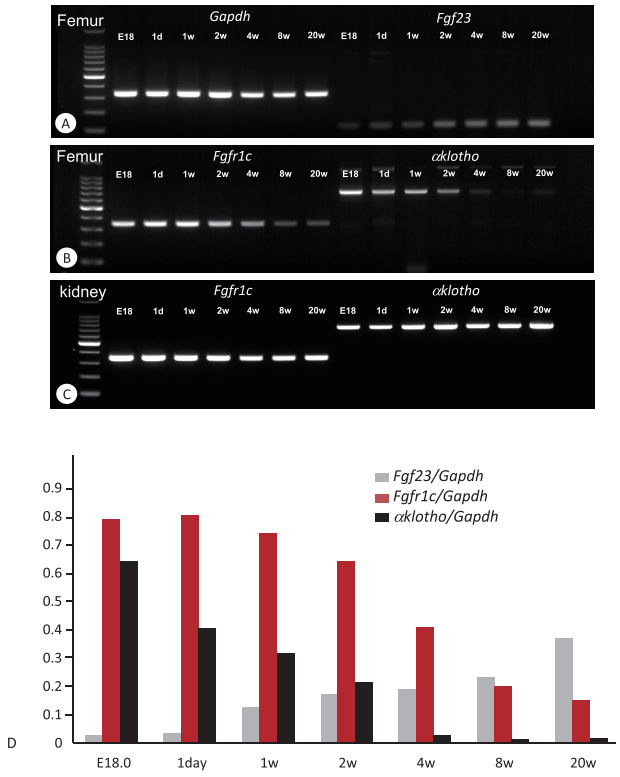

Fig. 5 RT-PCR analysis for gene expression of *Fgf23*, *Fgfr1c*, *αKlotho* and *Gapdh* in femur and kidney. Panels A shows RT-PCR products of chronological expression of *Gapdh* and *Fgf23*, and panel B are the gene expression of *Fgfr1c* and *αKlotho* in femur. In contrast, panel C is gene expression of *Fgfr1c* and *αKlotho* obtained from kidney. Panel D is the ratio of each gene expression standardized with the intensity of *Gapdh*. Note the chronological decrease of *Fgfr1c* and *αKlotho* genes, while the gradual increase of *Fgf23* in reverse.

and intense TNAP-immunoreactivity until 8 weeks-old, while sclerostin-immunoreactivity was hardly seen until 4 weeks-old, and then, came to be apparent after 8 weeks-old of age (see Figs. 2O and P). Unlike the close region, the distant region of trabeculae chronologically revealed a gradual increase of sclerostin-positive osteocytes (see Fig. 3O). It is well known that trabeculae close to the chondro-osseous junction, *i.e.*, primary trabeculae are the site of bone modeling in which osteoblasts are intensely activated even without osteoclasts. In contrast, the distant region of trabeculae is a site of bone remodeling coupled by osteoclastic activity. We have previously reported that the primary trabeculae showed an irregular distribution of osteocytes and their canaliculi, while the secondary trabeculae revealed a regular arrangement of osteocytes (13), and also demonstrated an intense sclerostin-immunoreactivity in osteocytes of the secondary trabeculae in adult mice (11). In addition, Kobayashi *et al.* documented that bone modeling mainly took place in the metaphyseal trabeculae at the embryonic and infant stages, however, bone remodeling gradually came to be predominant as an individual grew (17). Taken all together, we postulate that a different change of the index of sclerostin-positive osteocytes between the close and distant regions is dependent of the growth of mice and the site specificity—bone modeling site or bone remodeling site—.

Consistent with sclerostin, we have previously reported that FGF23 was synthesized in mature secondary and cortical bones, rather than immature primary trabeculae (37). However, in this study, FGF23 was observed in different cell-types—osteoblasts and osteocytes—during mice growth. *Fgf23* was seen in osteoblasts in the embryonic and neonatal stages, while the receptor, *Fgfr1c*/*αKlotho,* was strongly expressed in femora. This implies that FGF23 could function in an autocrine/paracrine manner in the fetal/neonatal stage of long bone. It was reported that before weaning, the vitamin D receptor is not expressed in intestine yet (27), and fetal kidney does not serve for mineral balance in serum due to the regulatory function of the fetal mineral metabolism in the placenta. Therefore, in the embryonic and neonatal stages, FGF23 synthesized in osteoblasts might be involved not in kidney-mediated serum concentration of phosphate and calcium, but in normal bone development. Meanwhile, one may wonder that the gene expression of *Fgf23* was not so high at the embryonic and neonatal stages, however, FGF23-immunoreactivity could be broadly and intensely found in both osteoblasts and osteocytes. The discrepancy between gene expression and immunoreactivity of FGF23 may be due to the possibility that FGF23 in embryonic and neonatal osteoblasts/osteocytes would not be secreted but accumulated inside the cells, or other reasons. We have previously examined bone mineralization in *kl/kl* mice in which the promoter region of *αKlotho* gene was disrupted and the transcription activities were extremely reduced. As a consequence, despite the high concentration of phosphate and calcium ions, defective bone mineralization was observed, indicating the possible mechanism of FGF23 signaling in autocrine/paracrine manner without mediating serum concentration of phosphate and calcium ions (30). If so, since *Fgf23* and *Fgfr1c*/*αKlotho* are shown to be expressed in the fetal and neonatal stages, it is of interest to examine what happens in fetal/neonatal bones of *kl/kl* mice, *αKlotho*$^{-/-}$ mice

and *Fgf23*$^{-/-}$ mice in future study.

In conclusion, our study provided histological evidences that sclerostin tends to be secreted in osteocytes of remodeled mature bone, while FGF23 would be differently synthesized in osteoblasts and osteocytes according to the developmental stages.

Acknowledgements

This study was partially supported by the Grants-in Aid for Scientific Research (Amizuka N, Hasegawa T), Promoting International Joint Research (Bilateral Collaborations) of JSPS and NSFC (Amizuka N, Li M).

DISCLOSURES

The authors have no financial conflicts of interest.

REFERENCES

1. ADHR Consortium (2000) Autosomal dominant hypophosphataemic rickets is associated with mutations in FGF23. *Nat Genet* **26**, 345–348.
2. Aarden EM, Burger EH and Nijweide PJ (1994) Function of osteocytes in bone. *J Cell Biochem* **55**, 287–299.
3. Amizuka N, Hasegawa T, Oda K, Luiz de Freitas PH, Hoshi K, Li M and Ozawa H (2012) Histology of epiphyseal cartilage calcification and endochondral ossification. *Front Biosci* **4**, 2085–2100.
4. Baron R, Vignery A and Horowits M (1983) Lymphocytes, macrophages and the regulation of bone remodeling. In: *Bone and Mineral Research Annual 2* (ed by Peck WA), pp175–243, Elservier Science, New York.
5. Burger EH and Klein-Nulend J (1999) Mechanotransduction in bone role of the lacuno-canalicular network. *FASEB J* **13**, 101–112.
6. Donahue HJ (2000) Gap junctions and biophysical regulation of bone cell differentiation. *Bone* **26**, 417–422.
7. Doty SB (1981) Morphological evidence of gap junctions between bone cells. *Calcif Tissue Int* **33**, 509–512.
8. Erben RG (1996) Trabecular and endocortical bone surfaces in the rat: modeling or remodeling? *Anat Rec* **246**, 39–46.
9. Frost HM (1964) Dynamics of bone remodeling. In: *Bone Biodynamics* (ed by Frost HM), pp315–333, Little Brown, Boston.
10. Frost HM (1969) Tetracycline-based histological analysis of bone remodeling. *Calcif Tissue Res* **3**, 211–237.
11. Hasegawa T, Amizuka N, Yamada T, Liu Z, Miyamoto Y, Yamamoto T, Sasaki M, Hongo H, Suzuki R, de Freitas PH, Yamamoto T, Oda K and Li M (2013) Sclerostin is differently immunolocalized in metaphyseal trabecules and cortical bones of mouse tibiae. *Biomed Res (Tokyo)* **34**, 153–159.
12. Hattner R, Epker BN and Frost HM (1965) Suggested sequential mode of control of changes in cell behaviour in adult bone remodelling. *Nature* **206**, 489–490.
13. Hirose S, Li M, Kojima T, de Freitas PH, Ubaidus S, Oda K, Saito C and Amizuka N (2007) A histological assessment on the distribution of the osteocytic lacunar canalicular system using silver staining. *J Bone Miner Metab* **25**, 374–382.
14. Hongo H, Sasaki M, Kobayashi S, Hasegawa T, Yamamoto T, Tsuboi K, Tsuchiya E, Nagai T, Khadiza N, Abe M, Kudo A, Oda K, de Freitas PHL, Li M, Yurimoto H and Amizuka N (2016) Localization of minodronate in mouse femora through isotope microscopy. *J Histochem Cytochem* **64**, 601–622.
15. Klein-Nulend J, van der Plas A, Semeins CM, Ajubi NE, Frangos JA, Nijweide PJ and Burger EH (1995) Sensitivity of osteocytes to biomechanical stress in vitro. *FASEB J* **9**, 441–445.
16. Knothe Tate ML, Adamson JR, Tami AE and Bauer TW (2004) The osteocyte. *Int J Biochem Cell Biol* **36**, 1–8.
17. Kobayashi S, Takahashi HE, Ito A, Saito N, Nawata M, Horiuchi H, Ohta H, Ito A, Iorio R, Yamamoto N and Takaoka K (2003) Trabecular minimodeling in human iliac bone. *Bone* **32**, 163–169.
18. Kurosu H, Ogawa Y, Miyoshi M, Yamamoto M, Nandi A, Rosenblatt KP, Baum MG, Schiavi S, Hu MC, Moe OW and Kuro-o M (2006) Regulation of fibroblast growth factor-23 signaling by klotho. *J Biol Chem* **281**, 6120–6123.
19. Kurosu H, Yamamoto M, Clark JD, Pastor JV, Nandi A, Gurnani P, McGuinness OP, Chikuda H, Yamaguchi M, Kawaguchi H, Shimomura I, Takayama Y, Herz J, Kahn CR, Rosenblatt KP and Kuro-o M (2005) Suppression of aging in mice by the hormone Klotho. *Science* **309**, 1829–1833.
20. Li X, Zhang Y, Kang H, Liu W, Liu P, Zhang J, Harris SE and Wu D (2005) Sclerostin binds to LRP5/6 and antagonizes canonical Wnt signaling. *J Biol Chem* **280**, 19883–19887.
21. Liu S, Guo R, Simpson LG, Xiao ZS, Burnham CE and Quarles LD (2003) Regulation of fibroblastic growth factor 23 expression but not degradation by PHEX. *J Biol Chem* **278**, 37419–37426.
22. Liu S, Gupta A and Quarles LD (2007) Emerging role of fibroblast growth factor 23 in a bone-kidney axis regulating systemic phosphate homeostasis and extracellular matrix mineralization. *Curr Opin Nephrol Hypertens* **16**, 329–335.
23. Masuki H, Li M, Hasegawa T, Suzuki R, Ying G, Zhusheng L, Oda K, Yamamoto T, Kawanami M and Amizuka N (2010) Immunolocalization of DMP1 and sclerostin in the epiphyseal trabecule and diaphyseal cortical bone of osteoprotegerin deficient mice. *Biomed Res (Tokyo)* **31**, 307–318.
24. Nabeshima Y and Imura H (2008) alpha-Klotho: a regulator that integrates calcium homeostasis. *Am J Nephrol* **28**, 455–464.
25. Nakatani T, Sarraj B, Ohnishi M, Densmore MJ, Taguchi T, Goetz R, Mohammadi M, Lanske B and Razzaque MS (2009) In vivo genetic evidence for klotho-dependent, fibroblast growth factor 23 (Fgf23)-mediated regulation of systemic phosphate homeostasis. *FASEB J* **23**, 433–441.
26. Oda K, Amaya Y, Fukushi-Irie M, Kinameri Y, Ohsuye K, Kubota I, Fujimura S and Kobayashi J (1999) A general method for rapid purification of soluble versions of glycosylphosphatidylinositol-anchored proteins expressed in insect cells: An application for human tissue-nonspecific alkaline phosphatase. *J Biochem* **126**, 694–699.
27. Pike JW, Donaldson CA, Marion SL and Haussler MR (1982) Development of hybridomas secreting monoclonal antibodies to the chicken intestinal 1 alpha,25-dihydroxyvitamin D3 receptor. *Proc Natl Acad Sci USA* **79**, 7719–7723.
28. Poole KE, van Bezooijen RL, Loveridge N, Hamersma H, Papapoulos SE, Löwik CW and Reeve J (2005) Sclerostin is a delayed secreted product of osteocytes that inhibits bone formation. *FASEB J* **19**, 1842–1844.
29. Quarles LD (2003) Evidence for a bone–kidney axis regulating phosphate homeostasis. *J Clin Invest* **112**, 642–646.

30. Sasaki M, Hasegawa T, Yamada T, Hongo H, de Freitas PH, Suzuki R, Yamamoto T, Tabata C, Toyosawa S, Yamamoto T, Oda K, Li M, Inoue N and Amizuka N (2013) Altered distribution of bone matrix proteins and defective bone mineralization in klotho-deficient mice. *Bone* **57**, 206–219.
31. Sasaki M, Hongo H, Hasegawa T, Suzuki R, Liu Z, de Freitas PHL, Yamada T, Oda K, Yamamoto T, Li M, Totsuka Y and Amizuka N (2012) Morphological aspects of the biological function of the osteocytic lacunar canalicular system and of osteocyte-derived factors. *Oral Sci International* **9**, 1–8.
32. Schneider CA, Rasband WS and Eliceiri KW (2012) NIH Image to ImageJ: 25 years of image analysis. *Nat Methods* **9**, 671–675.
33. Shapiro F (1997) Variable conformation of GAP junctions linking bone cells: a transmission electron microscopic study of linear stacked linear, curvilinear, oval, and annular junctions. *Calcif Tissue Int* **61**, 285–293.
34. Shimada T, Mizutani S, Muto T, Yoneya T, Hino R, Takeda S, Takeuchi Y, Fujita T, Fukumoto S and Yamashita T (2001) Cloning and characterization of FGF23 as a causative factor of tumor-induced osteomalacia. *Proc Natl Acad Sci USA* **98**, 5945–5946.
35. Silvestrini G, Ballanti P, Leopizzi M, Sebastiani M, Berni S, Di Vito M and Bonucci E (2007) Effects of intermittent parathyroid hormone (PTH) administration on SOST mRNA and protein in rat bone. *J Mol Histol* **38**, 261–269.
36. Tsuboi K, Hasegawa T, Yamamoto T, Sasaki M, Hongo H, de Freitas PH, Shimizu T, Takahata M, Oda K, Michigami T, Li M, Kitagawa Y and Amizuka N (2016) Effects of drug discontinuation after short-term daily alendronate administration on osteoblasts and osteocytes in mice. *Histochem Cell Biol* **146**, 337–350.
37. Ubaidus S, Li M, Sultana S, de Freitas PH, Oda K, Maeda T, Takagi R and Amizuka N (2009) FGF23 is mainly synthesized by osteocytes in the regularly distributed osteocytic lacunar canalicular system established after physiological bone remodeling. *J Electron Microsc (Tokyo)* **58**, 381–392.
38. Urakawa I, Yamazaki Y, Shimada T, Iijima K, Hasegawa H, Okawa K, Fujita T, Fukumoto S and Yamashita T (2006) Klotho converts canonical FGF receptor into a specific receptor for FGF23. *Nature* **444**, 770–777.
39. Van Bezooijen RL, Roelen BA, Visser A, van der Wee-Pals L, de Wilt E, Karperien M, Hamersma H, Papapoulos SE, ten Dijke P and Löwik CW (2004) Sclerostin is an osteocyte-expressed negative regulator of bone formation, but not a classical BMP antagonist. *J Exp Med* **199**, 805–814.
40. Veverka V, Henry AJ, Slocombe PM, Ventom A, Mulloy B, Muskett FW, Muzylak M, Greenslade K, Moore A, Zhang L, Gong J, Qian X, Paszty C, Taylor RJ, Robinson MK and Carr MD (2009) Characterization of the structural features and interactions of sclerostin: molecular insight into a key regulator of Wnt-mediated bone formation. *J Biol Chem* **284**, 10890–10900.
41. Weber TJ, Liu S, Indridason OS and Quarles LD (2003) Serum FGF23 levels in normal and disordered phosphorus homeostasis, *J Bone Miner Res* **18**, 1227–12234.
42. Winkler DG, Sutherland MK, Geoghegan JC, Yu C, Hayes T, Skonier JE, Shpektor D, Jonas M, Kovacevich BR, Staehling-Hampton K, Appleby M, Brunkow ME and Latham JA (2003) Osteocyte control of bone formation via sclerostin, a novel BMP antagonist. *EMBO J* **22**, 6267–6276.